QIRT'2022
10.21611/qirt.2022.2008
16th Quantitative InfraRed Thermography Conference

Laser Lock-in Thermography for Inspection of Silver-Sintered Die Attaches

by S. Panahandeh*, D. May*,**, C. Grosse-Kockert*, B. Wunderle**, and M. Abo Ras*

* Berliner Nanotest und Design GmbH, Volmerstraße 9b, 12489 Berlin, Germany, *panahandeh@nanotest.eu*
** Chemnitz University of Technology, Chemnitz, Germany

Abstract

In this study we demonstrate the capabilities of lock-in thermography (LIT) for the inspection of sintered chip interconnections. The laser LIT technology is used to detect delamination in the sintered layer between copper pad and SiC chip. This work will present a LIT system for the failure analysis (FA) without spray coating for industrial inspections of electronic components with thin layers, low emissivity surfaces, and high conductivity, which may produce thermal failure contrast even below noise level of the IR camera systems.

1. Introduction

LIT is a non-destructive and contactless technique for testing various types of specimens and can be used for FA of electronic components. A typical assembly for devices under test (DUT) consists of a thin semiconductor power device (transistor or diode) with thicknesses below 200 µm, the die attach layer (sintered or soldered) with a bond line thickness (BLT) around 5-50 µm and a direct copper bonded (DCB) or active metal braze (AMB) substrate with overall thickness of approximately 600-1200 µm. In some assemblies a thin pad usually of copper with thickness below 80 µm is sintered on the chip to prevent direct wire bonding. The challenge in inspections of these sintered and soldered chips or thin copper layers, are the low layer thicknesses of the dies and die attaches, low emissivity surfaces and a high thermal diffusivity of materials resulting in fast temperature equalization and low thermal failure contrast.

To detect a failure in sintered layers the industry is looking for alternatives to cost intensive X-ray methods [1,2] and the time-consuming scanning acoustic microscopy (C-SAM) [3]. In contrast to earlier thermal FA techniques, like pulsed infrared thermography (PIRT), LIT can be applied for samples with low emissivity surfaces without any sample preparation like temporary lamination or spray coating [4,5]. Furthermore, the temperature resolution of PIRT is in the order of 100 mK, which is not sufficient for sample surfaces with low emissivity and high conductivity, which may produce temperature contrast well below 1 mK. This work will present LIT with laser excitation as a quality assessment tool to perform reliable inspections on silver-sintered die attaches. Furthermore, hardware and measurement parameter specifications for the IR failure analysis system are defined.

2. Sample Design

Power components such as MOSFETs, IGBT transistors and freewheeling diodes are impacted by die attach both mechanically and thermally. The performance of a component or module may be seriously compromised whenever a crack, a delamination, or a void develops here. Thus, its reliability cannot be guaranteed. Therefore, it is important to identify and reject these defects during the production. Silver-sinter plays a significant role in the increasing volume of power modules used for renewable energies and e-mobility. Among the principle reasons for replacing soldered layers with silver-sintered layers is their higher thermal conductivity (151.6 W/m.K for a sintered silver sample with 22% of porosity [6]). Figure 1 shows an exemplary cross-section of such assembelies. Sintering paste is used to apply a copper pad to a SiC chip and to bond the chip to a substrate. Copper pad is added to this assembly to prevent direct wire bonding on the chip. During wire bonding, copper pad absorbs the high mechanical load and keep the chip from being damaged. In addition, it ensures an even distribution of current across the chip. Thickness of copper pad, sintered layer, chip, and substrate are, 60 µm, 25 µm, 120 µm, and 1200 µm, respectively. The DCB substrate, consists of an electrically non-conductive ceramic, often a Si_3N_4 ceramic, and copper layers applied on both sides. The main focus of this paper is to detect delamination in the sintered layer on top of the chip.

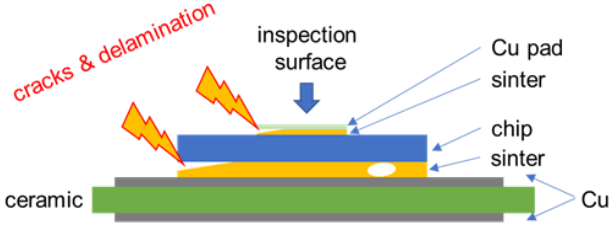

Fig. 1. *Principle package in cross-section including cracks and delamination in sintering layers between chip and substrate as well as chip and copper pad.*

3. Experimental Setup

Figure 2 shows a schematic overview of the laser LIT experimental setup. The setup consists of an IR camera, which can detect IR wavelengths in the spectral range of 3 – 5 µm, a 450 nm diode laser with 5 W optical output, and some optical components to convert the output of the laser to a homogeneous beam and to match it to the size of the DUT surface. In order to perform LIT, IR camera and laser are connected to a control box which synchronizes laser pulses and image capture with the lock-in frequency. In LIT the surface of the DUT is periodically thermally excited and the thermal waves propagate through the material [7]. The amplitude and phase information of these waves are influenced by the internal structure of the object. The IR camera records the oscillation temperature field during the measurement. Depending on the temperature resolution of the measuring system, the information sought may initially be lost in the noise of the measuring system. The data will be lock-in amplified to acquire useful signals with an amplitude smaller than the noise amplitude of a measurement signal and in case of a defect in the DUT the temperature contrast can be detected.

The Fourier analysis can be performed at each pixel of the temperature field which is recorded during the modulated illumination with an IR camera and the results can be shown as amplitude and phase images.

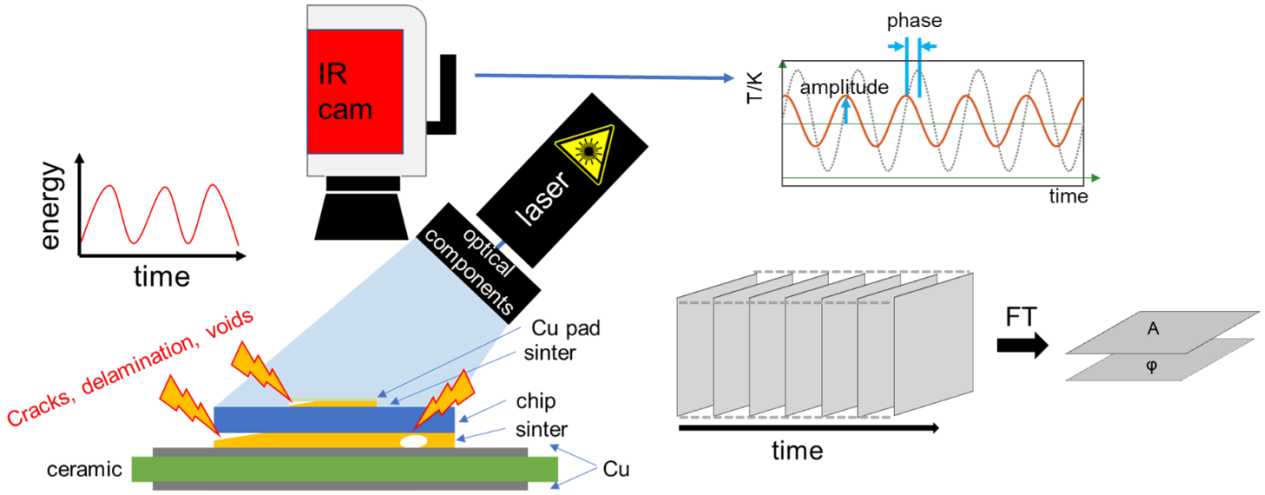

Fig. 2. *Measurement principle and experimental setup of the laser lock-in thermography. The device under test, which includes a defect, is periodically thermally excited through the external light. The light is generated by a laser source. The IR camera records the oscillation temperature field through the experiment. An amplitude and phase estimate of the thermal wave response is obtained using Fourier analysis.*

LIT compared to PIRT provides lower thermal load to the DUT and the option to select the depth of interest. In addition, in LIT the noise amplitude is decreased continuously with each excitation period (N) proportional to the square root of the excitation periods (~1/sqrt(N)). That means to decrease the noise by a factor two, four times of the excitation periods are necessary. However, the measurement time is longer than PIRT, and each measurement is optimized for only one penetration depth. Laser LIT uses a modulated continuous wave (CW) laser as the heat source. The principle significant benefits of lasers are that they have a monochromatic emission spectrum and there is the possibility to achieve higher modulation frequencies. With laser beams, a selected and relatively small surface can be heated directly, and moreover scanning laser heat sources can be used to inspect large structures. Due to the directivity and low energy loss of the lasers compared to normally utilized halogen and flash lamps, they can be precisely positioned at great distances from the target structure. Thermal wave fields can be measured without special surface alteration [8].

4. Methodology

The propagation of thermal waves within the surrounding material can be determined by a periodic heat source simulation. These waves are highly damped and exhibit frequency dependence [9]. The stationary oscillating temperature field as a function of depth *z* and time *t* can be described with Eq. (1)

$$T(z,t) = T_0 \cdot \ e^{-z/\mu} \cdot \ cos\left(2\pi \cdot f \cdot t - \frac{2\pi \cdot z}{\lambda}\right) \tag{1}$$

where *f* is excitation frequency, λ thermal wavelength, and μ thermal diffusion length. The equation consists of a cosine-term that generates the oscillation with a depth- and wavelength dependent phase. Similarly, it has an *e*-function damped by depth and diffusion length. The diffusion length and thermal wavelength are defined as Eqs. (2) and (3)

$$\mu = \sqrt{\frac{k}{\pi \cdot f \cdot \rho \cdot c_p}} = \sqrt{\frac{\alpha}{\pi \cdot f}} \tag{2}$$

$$\lambda = 2\pi \cdot \mu \tag{3}$$

with thermal conductivity k, density ρ, specific heat capacity c_p, thermal diffusivity α. Eq. (2) shows the penetration depth of a thermal wave can be increased by decreasing the frequency or with increasing the diffusivity.

A thermal wave is reflected on interfaces of different materials just like any other wave, for example, an acoustic wave in ultrasonic microscopy. *Bertolotti* described the reflected and transmitted thermal wave generally and has demonstrated them experimentally in [10]. The reflection coefficient (R) at the interface of two materials 1 and 2 can be written as:

$$R = \frac{b-1}{b+1} \tag{4}$$

$$b = \frac{\sqrt{k_2 \cdot \rho_2 \cdot c_2}}{\sqrt{k_1 \cdot \rho_1 \cdot c_1}} \tag{5}$$

R stands between 0 and 1, and it is, for example, particularly large at the interface between a die attach layer and a void inside the die attach. Thus, thermal waves, as well as thermal pulses, are useful for detecting voids, delamination, and cracks.

Eq. (2) shows that the diffusion length is inversely proportional to the excitation frequency. Hence, thermal waves can only penetrate a material deeper at lower frequencies. Table 1 gives an overview of thermal material data and penetration depths for different frequencies and relevant materials. The typical frequency range is from a few mHz to around 10 Hz. Materials like thermally slow moulding compounds (MC) require low frequency and materials like copper and aluminium require higher frequencies.

***Table 1**: Overview of thermal material data, as well as diffusion and thermal wavelengths of selected materials [9,11].*

Material	***k*** **[W/(m.K)]**	c_p **[J/(kg.K)]**	ρ **[kg/m³]**	α **[m²/s]**	μ **@ *5* Hz [mm]**	μ **@ *1* Hz [mm]**	μ **@ 0.2 Hz [mm]**
Moulding Compound	0.6	1070	1810	3.1E-7	0.083	0.186	0.416
Air	0.026	1007	1.1614	222.3E-7	1.19	2.66	5.95
Solder	35	129	11336	2.4E-5	1.24	2.76	6.18
Aluminium	155	875	2770	6.4E-5	2.02	4.51	10.1
Silicon	148	712	2330	8.9E-5	2.01	4.49	10.0
Copper	372	419	8827	1.0E-4	2.53	5.66	12.65
Silver	427	235	10500	1.7E-4	3.29	7.36	16.45

The phase velocity of thermal wave v is defined according to Eq. (6) and shows the phase velocity can be increased with increasing frequency or diffusivity. The equation can be used to calculate the time when the wave front reaches a certain depth. It is also possible to determine the depth of an inhomogeneity under certain conditions when the wavefront is reflected.

$$v = \lambda \cdot f = 2\sqrt{\pi \cdot \alpha \cdot f} \tag{6}$$

Temperature resolution which can be detected using LIT is down to µ-mK range. *Breitenstein* achieved temperature resolutions of up to 10 µK and shows the high potential for a lateral high-resolution (5 µm) method for defect localization [12,13]. *Rakotoniaina* detects temperature signals of 40 µK triggered by short circuits in solar cells after 1000 seconds of measurement [14].

When the excitation frequency is selected such that the wave penetrates to the depth of defect, the detectability will be further affected by the following factors:

A. Wavelength and power of the Laser

Based on the wavelength of the laser light and power of the laser used, thermal contrast can be manipulated. Various metals show totally different absorption behaviour in optical frequency spectrum. Aluminium significantly absorbs wavelengths shorter than 100 nm, whereas gold and silver are kind of sensitive to the wavelength 300-500 nm, and steel and pure iron to wavelengths more than 1050 nm. Copper absorbs more than 50 percent of incident light at blue light wavelengths, while at infrared wavelengths, it absorbs only about five percent.

The thermal contrast can be increased with higher excitation pulse power. It should be noticed that it cannot be increased arbitrarily since it causes destruction of the surface.

B. Surface Property

Modern thermal cameras are capable of detection a temperature difference down to 20 mK and images are primarily generated via thermal radiation. Depending on the temperature (*T*), an object's radiated power (P_{rad}) can be described by the Stefan-Boltzmann law:

$$P_{rad} = \varepsilon \cdot \sigma \cdot A \cdot T^4 \tag{7}$$

where ε is the emissivity, σ the Stefan-Boltzmann constant, and *A* the surface area. Based on Eq. (7), the amount of radiation emitted depends on the emissivity of a surface. The emissivity is specified normalized to the black body with values between 0 and 1. Table 2 lists important materials with associated emissivity.

Table 2: *Overview of emissivity of selected materials [15]*

Material	Temperature [°C]	Emissivity	Material	Temperature [°C]	Emissivity
Aluminium polished oxidized anodized	 50-100 50-500 100	 0.04-0.06 0.2-0.3 0.55	Copper polished oxidized	 100 50	 0.03 0.7
Moulding Compound	-	0.80-0.95	Silver polished	 200-600	 0.02-0.03
Nickel polished oxidized	 20 200-600	 0.05 0.37-0.48	Solder oxidized shiny	 20 250	 0.28 0.08

C. IR Camera

A wide assortment of IR cameras is available which are different as far as their thermal resolutions, spatial resolutions, frame rates, and costs. An IR camera basically comprises of an optic, a detector, and the readout electronics, which are completely consolidated in one housing. The Noise Equivalent Temperature Difference (NEDT) demonstrates the smallest measurable temperature contrast, which can be detected. This value represents the amount of radiation needed to overcome the intrinsic noise of the detector and generate the temperature measurement signal. It relies upon the average object temperature which should subsequently be determined. Common qualities for uncooled thermal detectors are 80 mK at 30 °C. Noise mainly results from thermal fluctuations, but there are also sources of noise from changes in temperature in the detector, as well as background noise provided by radiative heat exchange between the detector and the environment [11].

Breitenstein gives Eq. (8) for predicting the mean noise amplitude A_{noise} [16]. The noise level does not depend on the lock-in frequency, but only on the frame rate of the IR camera f_s and the duration of the measurement t_{meas}, as well as the NEDT of the IR camera.

$$A_{noise} = \frac{2}{\sqrt{f_s \cdot t_{meas}}} \cdot NEDT \tag{8}$$

May [15] shows for cooled InSb detectors longer integration times and higher object temperatures can both reduce the NEDT and the noise amplitude. During an experiment he shows that by increasing the mean object temperature from 32.7 °C to 82.8 °C, the NEDT has been decreased from 47 mK to 20 mK. The reason is the impressive increase (by the 4th power) of the IR signal according to (cf. Stefan-Boltzmann law, Eq. (7)), combined with the improvement of the SNR of the IR detector.

5. Results

Figure 3 shows a 3 x 3 mm² copper pad sintered to SiC chip with artificial defect in the sintered layer (see figure 1). The frequency modulation of the laser was 1 Hz during the measurement. The first three images of figure 3 contain results from LIT (live, amplitude, and phase images, respectively), and the last one shows result from C-SAM as a reference for comparison. The enclosed area in the yellow curve at the phase and C-SAM images show delamination in the sintering layer between copper pad and the chip. Thermal signature is sometimes dominated by polyimide frame (enclosed area between two red rectangles). The amplitude image is sensitive to disturbing surface defects, reflections, and distribution of optical illumination (shown with white arrows in the amplitude image) while in the phase image each of these effects is eliminated during the evaluation.

Figure 4 shows seven additional samples similar to that in figure 3. Results from LIT are shown in the first three rows (live, amplitude, phase), while C-SAM results are shown in the last row. In the measurements, the presented LIT system could detect thermal contrast signals of 15 mK, which is below the noise level of the IR-camera (80 mK). However, further investigations are necessary to determine the smallest detectable temperature contrast. The average phase contrast between defective and non-defective area is 15 degrees. The phase results demonstrate that the samples have delamination in the sintered layer between the copper pads and chips. The measurements show that the phase results have a good agreement to results obtained by C-SAM and can detect inhomogeneous temperature distribution in the sinter area. It should be considered that C-SAM images also show the structural information of the sinter material which do not necessarily affect the thermal performance of a module. The measurement time for LIT is 15 s for each chip.

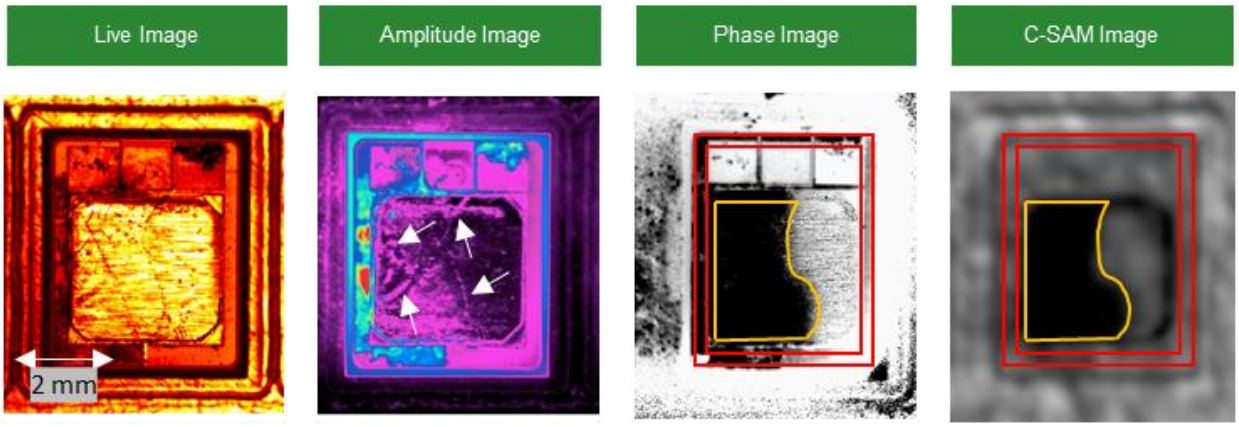

Fig. 3: *Image analysis of 3 x 3 mm² copper pad sintered to the SiC chip with artificial defect in the sintered layer similar to that shown in figure 1. Live, amplitude, and phase images of lock-in IR thermography with laser excitation (first three right images), C-SAM image (left). White arrows in amplitude image mark the surface scratches on the copper pad. The delamination and polyimide areas in phase and C-SAM images are marked in yellow and red, respectively.*

6. Conclusions

LIT can detect defects such as voids, cracks, and delamination in silver-sintered layers without any sample preparation. The important advantage of using LIT compared to PIRT is the capability to detect defects in samples, which may produce temperature contrast well below 1 mK.

The paper presents a LIT system which can be used for evaluation and testing of specimens such as electronic components with thin layers, low emissivity surfaces, and high conductivity materials during production, and is suitable for 100% inspection in production lines.

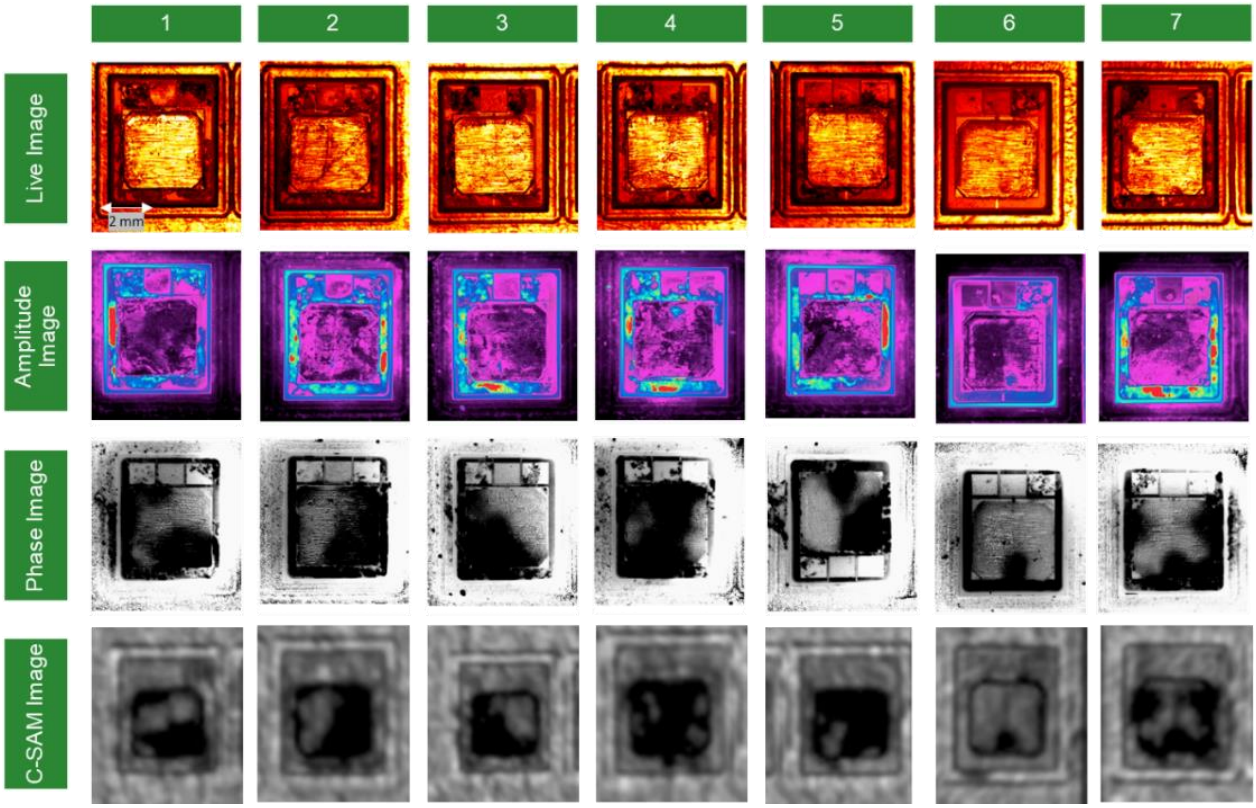

Fig. 4. *Seven samples similar to that shown in figure 3. The first three rows contain results (live, amplitude, and phase images, respectively) of lock-in IR thermography with laser excitation and the last row shows the C-SAM results.*

REFERENCES

[1] Pacheco, Mario, and Deepak Goyal. "X-ray computed tomography for non-destructive failure analysis in microelectronics." 2010 IEEE International Reliability Physics Symposium. IEEE, 2010.

[2] Pacheco, Mario, and Deepak Goyal. "Detection and characterization of defects in microelectronic packages and boards by means of high-resolution X-ray computed tomography (CT)." 2011 IEEE 61st Electronic Components and Technology Conference (ECTC). IEEE, 2011.

[3] Hartfield, Cheryl D., and Thomas M. Moore. "Acoustic Microscopy of Semiconductor Packages." Microelectronics Failure Analysis Desk Reference, 2011.

[4] Panahandeh, S., D. May, D. R. Wargulski, E. Boschman, R. Schacht, M. Abo Ras, and B. Wunderle. "Infrared thermal imaging as inline quality assessment tool." In 2021 22nd International Conference on Thermal, Mechanical and Multi-Physics Simulation and Experiments in Microelectronics and Microsystems (EuroSimE), pp. 1-6. IEEE, 2021.

[5] Panahandeh, S., D. May, C. Grosse-Kockert, A. Stelzer, B. Rabay, D. Busse, B. Wunderle, and M. Abo Ras. "Inline failure analysis of sintered layers in power modules using infrared thermography." In 2022 23rd International Conference on Thermal, Mechanical and Multi-Physics Simulation and Experiments in Microelectronics and Microsystems (EuroSimE), pp. 1-7. IEEE, 2022.

[6] Ordonez-Miranda, Jose, Marrit Hermens, Ivan Nikitin, Varvara G. Kouznetsova, and Sebastian Volz. "Modeling of the effective thermal conductivity of sintered porous pastes." In 20th International Workshop on Thermal Investigations of ICs and Systems, pp. 1-4. IEEE, 2014.

[7] Wargulski, D. R., D. May, C. Grosse-Kockert, E. Boschman, B. Wunderle, and M. Abo Ras. "Inspection of silver-sinter die attaches by pulsed and lock-in infrared thermography with flash lamp and laser excitation." In 15th Quantitative InfraRed Thermography Conference, pp. 21-30, 2020.

[8] An, Yun-Kyu, Ji Min Kim, and Hoon Sohn. "Laser lock-in thermography for detection of surface-breaking fatigue cracks on uncoated steel structures." Ndt & E International 65, 54-63, 2014.

[9] May, Daniel, Bernhard Wunderle, Ralph Schacht, and Bernd Michel. "Transient thermal response as failure analytical tool-a comparison of different techniques." In 2013 14th International Conference on Thermal, Mechanical and Multi-Physics Simulation and Experiments in Microelectronics and Microsystems (EuroSimE), pp. 1-5. IEEE, 2013.

[10] Bertolotti, M., G. L. Liakhou, R. Li Voti, S. Paoloni, and C. Sibilia. "Thermal wave reflection and refraction: Theoretical and experimental evidence." Journal of applied physics 85, no. 7: 3540-3545, 1999.

[11] May, D. "Transiente Methoden der Infrarot-Thermografie zur zerstörungsfreien Fehleranalytik in der mikroelektronischen Aufbau-und Verbindungstechnik." Doctoral thesis, TU Chemnitz, 2015.
[12] Breitenstein, O., M. Langenkamp, J. Zettner, and C. Peppermüller, “Hochempfindliche lock-in thermographie zur abbildung von \muW-wärmequellen,”, 2002.
[13] Breitenstein, O., J. P. Rakotoniaina, F. Altmann, J. Schulz, and G. Linse. "Fault localization and functional testing of ICs by lock-in thermography." In ISTFA 2002, pp. 29-36. ASM International, 2002.
[14] Rakotoniaina, J. P., O. Breitenstein, and M. Langenkamp. "Localization of weak heat sources in electronic devices using highly sensitive lock-in thermography." Materials Science and Engineering: B 91: 481-485, 2002.
[15] Maldague, Xavier. "Theory and practice of infrared technology for nondestructive testing.", 2001.
[16] Breitenstein, Otwin, Wilhelm Warta, and Martin Langenkamp. Lock-in thermography: "Basics and use for evaluating electronic devices and materials. " Vol. 10. Berlin: Springer, 2010.